SUPPORTING INFORMATION

Fluorescein: a Photo-CIDNP Sensitizer Enabling Hyper-Sensitive NMR Data Collection in Liquids at Low Micromolar Concentration

Yusuke Okuno and Silvia Cavagnero

Department of Chemistry, University of Wisconsin - Madison, 1101 University Ave., Madison, Wisconsin, 53706, USA

Correspondence should be addressed to S.C. (Email: cavagnero@chem.wisc.edu, Phone: 608-262-5430).

Supporting Experimental Methods

Kinetic Simulations. Most of the steady-state triplet state concentrations of FL were calculated either exactly or approximately by solving eq. (4) and eq. (44) using MATLAB (The MathWorks Inc. Natick, MA, version 2014a). The integral in eq. (48), (50) and (53) were carried out with MATLAB as finite summations. The time course of the FL dye T1 triplet concentration (Fig. S3), and the steady-state triplet dye concentrations as a function of total dye concentration in the presence of 10 μM Trp (Fig. S4) were generated with the Gepasi kinetic-simulation software (version 3.30)[1].

General aspect of kinetic-model design. To help explain the origin of the excellent photo-CIDNP sensitivity enhancement displayed by the photo-sensitizer dye fluorescein dianion (FL) at low NMR-sample concentration (low micromolar Trp in the present study), we computed the expected triplet-state dye concentration according to the reaction scheme of Figure 5a. Our experiments employed catalytic amounts of glucose oxidase (GO) and catalase (CAT), two enzymes known to reduce the concentration of oxygen in solution down to low micro molar concentration[2]. These enzymes have already been successfully used in the context of photo-CIDNP[3]. Although even small amounts of residual oxygen may lead to significant FL triplet-state depopulation, this effect was neglected in the simulations. In general, the simulations neglected any irreversible photo-degradative process, on the grounds that single-scan experiments with continuous laser irradiation time of 0.1 s (1.5 W), did not lead to any significant reduction in the amount of FL or Trp in solution. Some of the rate constants pertaining to relevant kinetic steps were not available in the literature, to the best of our knowledge. For these rate constants we deduced pertinent values from theory (see below). Given the above assumptions, the kinetic simulations should not be regarded as quantitative. Yet, their semi-quantitative nature renders them instrumental to highlight expected leading trends.

Rationale for the analysis of triplet state dye concentrations under steady-state conditions. Although the triplet-state dye concentration depends on laser irradiation time (we used 0.1 s argon-ion laser in multiline mode (main line 488 and 514 nm) , 1.5 W laser power), the simulations showed that the actual FL triplet state concentration reaches a steady-state value very fast (i.e., within 0.01 s) relative to the continuous laser irradiation time (See Fig. S3). Hence we elected to predict triplet-state steady-state dye concentrations, and regard them as good reporters for the actual amount of triplet-state dye to be expected in the experiments.

Prediction of steady-state triplet-state dye concentrations in the low-Trp-concentration limit. In the low-Trp concentration limit, we analyzed the limiting case of $[Trp]_{TOT}$ =

0. Under steady-state conditions, it is possible to calculate the steady-state triplet concentration of FL analytically, and thus analyze how each rate constant contributes to determine triplet-state dye concentrations.

The kinetics of each electronic state of the dye, including self triplet quenching are described by

$$\frac{d[^{S_0}D(t)]}{dt} = -k_{ex}[^{S_0}D(t)]+k_{TS}[^{T_1}D(t)]+k_{fl}[^{S_1}D(t)]+k_{q,tt}[^{T_1}D(t)][^{T_1}D(t)]+k_{q,ts}[^{T_1}D(t)][^{S0}D(t)] \quad (1)$$

$$\frac{d[^{S_1}D(t)]}{dt} = -(k_{isc}+k_{fl})[^{S_1}D(t)]+k_{ex}[^{S_0}D(t)] \quad , \quad (2)$$

$$\frac{d[^{T_1}D(t)]}{dt} = k_{isc}[^{S_1}D(t)]-k_{TS}[^{T_1}D(t)]-k_{q,tt}[^{T_1}D(t)][^{T_1}D(t)]-k_{q,ts}[^{T_1}D(t)][^{S0}D(t)] \quad , \quad (3)$$

where $[^{S0}D(t)]$, $[^{S_1}D(t)]$ and $[^{T_1}D(t)]$ are the time-dependent concentrations of ground, first singlet, and triplet states, respectively. Notation for the rate constants are described in Table 1.

The steady-state concentration of the triplet state ($[^{T_1}D]$) is obtained upon setting eqns. (1)-(3) to zero. The $[^{T_1}D]$ is then deduced as

$$[^{T_1}D] = \frac{-B+\sqrt{B^2+4C}}{2C}k_{isc}[D]_{TOT} \quad , \quad (4)$$

where $[D]_{TOT}$ is the initial concentration of the dye, and the A-C constants are defined as $A = \frac{(k_{fl}+k_{isc})}{k_{ex}}$, $B=\left\{A(k_{TS}+k_{q,ts}[D]_{TOT})+k_{TS}+k_{isc}\right\}$, and

$C=\left\{A(k_{q,tt}-k_{q,ts})+k_{tt}\right\}k_{isc}[D]_{TOT}$.

Steady-state triplet dye concentration in the presence of Trp. In the presence of significant concentrations of Trp, all the steps of Figure 5a are relevant, and were employed to calculate the steady-state triplet state dye concentration. The time-dependent population of each state is described by

$$\frac{d[^{S_0}D(t)]}{dt} = -\left(k_{ex}+k_a[Trp(t)]\right)[^{S_0}D(t)]+k_d[(^{S_0}DTrp)(t)]+k_{fl}[^{S_1}D(t)]+k_{TS}[^{T_1}D(t)]$$
$$+k_{q,tt}[^{T_1}D(t)][^{T_1}D(t)]+k_{q,ts}[^{T_1}D(t)][^{S0}D(t)] \quad , \quad (5)$$

$$\frac{d[^{S_1}D(t)]}{dt} = -(k_{isc}+k_{fl})[^{S_1}D(t)]+k_{ex}[^{S_0}D(t)] \quad , \tag{6}$$

$$\frac{d[^{T_1}D(t)]}{dt} = k_{isc}[^{S_1}D(t)] + k_d[(^{T_1}DTrp)(t)] - \left(k_{TS}+k_a[Trp(t)]\right)[^{T_1}D(t)]$$

$$-k_{q,tt}[^{T_1}D(t)][^{T_1}D(t)] - k_{q,ts}[^{T_1}D(t)][^{S0}D(t)] \quad , \tag{7}$$

$$\frac{d[(^{T_1}DTrp)(t)]}{dt} = k_a[Trp(t)][^{T_1}D(t)] - \left(k_d+k_{et}\right)[(^{T_1}DTrp)(t)] \quad , \tag{8}$$

$$\frac{d[^{S}RP(t)]}{dt} = k_{a1}[Trp^{\bullet+}(t)][D^{\bullet-}(t)] + k_{mix}[^{T_0}RP(t)] - \left(k_{mix}+k_{d1}+k_{bet}\right)[^{S}RP(t)] \quad , \tag{9}$$

$$\frac{d[^{T_0}RP(t)]}{dt} = k_{a1}[Trp^{\bullet+}(t)][D^{\bullet-}(t)] + \frac{k_{et}}{3}[(^{T}DTrp)(t)]+k_{mix}[^{S}RP(t)]$$

$$-\left(k_{mix}+k_{d1}\right)[^{T_0}RP)(t)] \quad , \tag{10}$$

$$\frac{d[^{T_{\pm1}}RP(t)]}{dt} = k_{a1}[Trp^{\bullet+}(t)][D^{\bullet-}(t)] + \frac{k_{et}}{3}[(^{T_{\pm}}DTrp)(t)] - k_{d1}[^{T_{\pm}}RP(t)] \quad , \tag{11}$$

$$\frac{d[(^{S_0}DTrp)(t)]}{dt} = k_{bet}[^{S}RP(t)] - k_d[(^{S_0}DTrp)(t)]+k_a[Trp(t)][^{S_0}D(t)] \quad , \tag{12}$$

$$\frac{d[D^{\bullet-}(t)]}{dt} = k_{d1}[RP(t)] - k_{a1}[Trp^{\bullet+}(t)][D^{\bullet-}(t)] \quad . \tag{13}$$

The steady state concentration of $[^{T_1}D]$ was computed upon setting each of eqs. (5) – (13) equal to zero, after considering the mass-conservation relations

$$[D]_{TOT} = [^{S_0}D(t)]+[^{S_1}D(t)]+[^{T_1}D(t)]+[RP(t)]+[D^{\bullet-}(t)]+[(^{T_1}DTrp)(t)]+[(^{S_0}DTrp)(t)] \quad , \tag{14}$$

and

$$[Trp]_{TOT} = [Trp(t)]+[RP(t)]+[Trp^{\bullet+}(t)]+[(^{T_1}DTrp)(t)]+[(^{S_0}DTrp)(t)] \quad . \tag{15}$$

Upon noting that, at all times, [Trp]>>[T], one can regard the bimolecular reaction involving Trp as a pseudo-first order process, by setting the steady state concentration of Trp as $[Trp] \cong [Trp]_{TOT}$. Then, after a few algebraic steps, one obtains

$$A_1 = \frac{k_{isc}+k_{fl}}{k_{ex}} \quad , \tag{16}$$

$$A_2 = \frac{k_a[\mathrm{Trp}]}{k_{et} + k_d} \quad , \tag{17}$$

$$A_3 = k_{TS} + k_a[\mathrm{Trp}] - k_d A_2 \quad , \tag{18}$$

$$A_4 = 1 + A_1\left(1 + \frac{k_a}{k_d}[\mathrm{Trp}]\right) \quad , \tag{19}$$

$$A_5 = \frac{2}{3}k_{et}\left(1 + \frac{k_{d1}}{2k_{d1} + 2k_{mix}}\right) \quad , \tag{20}$$

$$A_6 = -A_5 k_{a1}\left(2 + \frac{k_{d1}}{k_{d1} + k_{mix}}\right) \quad , \tag{21}$$

$$A_7 = A_5 k_{d1} \quad , \tag{22}$$

$$A_8 = -A_5 k_{d1}\left(1 + \frac{k_{mix}}{k_{d1} + k_{mix}}\right) \quad , \tag{23}$$

$$A_9 = \frac{k_{d1}}{4k_{a1}} \frac{4k_{a1} + k_{et}A_6 - k_{d1} + k_{et}A_7}{k_{et}A_8 - k_{bet}} \quad , \tag{24}$$

$$A_{10} = 1 + A_7\left(1 + \frac{k_{et}}{k_d} + \frac{k_{et}}{A_9 k_{bet}}\right) \quad , \tag{25}$$

$$A_{11} = \frac{k_{d1}}{k_{a1}} \frac{k_{et}}{k_{bet}} A_2 \quad , \tag{26}$$

$$B_1 = \left(A_4 k_{q,tt}\right)^2 \quad , \tag{27}$$

$$B_2 = 2k_{q,tt}\left(A_4\right)^2 A_3 \quad , \tag{28}$$

$$B_3 = \left(A_3 A_4\right)^2 \quad , \tag{29}$$

$$B_4 = -2k_{q,tt}k_{q,ts}A_1 A_4 A_{10} \quad , \tag{30}$$

$$B_5 = 2A_4 k_{q,tt} k_{isc} A_5 - 2A_4 A_1 k_{q,ts}\left(A_3 A_5 - k_{q,tt}[\mathrm{D}]_{TOT}\right) \quad , \tag{31}$$

$$B_6 = 2A_4\left(k_{isc}\left(A_3A_5 - k_{q,tt}[D]_{TOT}\right) + k_{q,ts}A_1A_3[D]_{TOT}\right) \quad , \tag{32}$$

$$B_7 = -2k_{isc}A_4A_3[D]_{TOT} \quad , \tag{33}$$

$$C_1 = \left(k_{q,ts}A_1A_{10}\right)^2 \quad , \tag{34}$$

$$C_2 = -\left(k_{q,ts}A_1\right)^2\left(2A_{10}[D]_{TOT} + A_{11}\right) - 2k_{isc}k_{q,ts}A_1\left(A_{10}\right)^2 \quad , \tag{35}$$

$$C_3 = \left(k_{q,ts}A_1\right)^2\left([D]_{TOT}\right)^2 + 2k_{isc}k_{q,ts}A_1\left(2A_{10}[D]_{TOT} + A_{11}\right) + \left(k_{isc}\right)^2\left(A_{10}\right)^2 \quad , \tag{36}$$

$$C_4 = -2k_{isc}k_{q,ts}A_1\left([D]_{TOT}\right)^2 - \left(k_{isc}\right)^2\left(2A_{10}\left([D]_{TOT}\right)^2 + A_{11}\right) \quad , \tag{37}$$

$$C_5 = \left(k_{isc}[D]_{TOT}\right)^2 \quad , \tag{38}$$

$$A = B_1 + B_4 + C_1 \quad , \tag{39}$$

$$B = B_2 + B_5 + C_2 \quad , \tag{40}$$

$$C = B_3 + B_6 + C_3 \quad , \tag{41}$$

$$D = B_7 + C_4 \quad , \tag{42}$$

$$E = C_5 \quad , \tag{43}$$

and finally

$$A[{}^{T_1}D(t)]^4 + B[{}^{T_1}D(t)]^3 + C[{}^{T_1}D(t)]^2 + D[{}^{T_1}D(t)] + E = 0 \, . \tag{44}$$

Eq. (44) was solved with MATLAB. This approximation works well as shown in Fig. S4, which illustrates the fact that simulations with no approximations (using the Gepasi software) and simulations that include the above approximation are superimposable.

Association and dissociation rate constants were regarded as equivalent, for ${}^{S}RP$, ${}^{T0}RP$, ${}^{T+}RP$ and ${}^{T-}RP$, according to relations

$$k_{a1,T_-} = k_{a1,T_0} = k_{a1,T_+} = k_{a1,S} = k_{a1} \quad , \tag{45}$$

$$k_{a1,tot} = k_{a1,T_-} + k_{a1,T_0} + k_{a1,T_+} + k_{a1,S} = 4k_{a1} \quad , \tag{46}$$

$$k_{d1,T_-} = k_{d1,T_0} = k_{d1,T_+} = k_{d1,S} = k_{d1} \quad . \tag{47}$$

We assumed that intersystem crossing rate constants are equal for all triplet sublevels.

$$k_{isc,T_-} = k_{isc,T0} = k_{isc,T_+} = \frac{k_{isc}}{3} \quad , \tag{48}$$

This is a reasonable 1st order approximation given that internal spin orbit interactions are probably not significantly affected by the applied magnetic field, and that spin-spin interactions play a negligible role at high magnetic field, yielding any electron spin polarization[4]. The triplet-state energies are non-degenerate, in the presence of the applied magnetic field. On the other hand, we assumed that the energy splitting is very small, and that the relevant density of states are not significantly affected by the applied magnetic field.

Additional comments on the extinction-coefficient-dependence simulations of Figure 6. We estimated steady-state ^{T1}D concentrations at very low Trp concentration, down to 0.1 μM. At this low Trp concentration value, one may think that the pseudo-first order approximation ($[Trp] \cong [Trp]_{TOT}$) is not applicable, given that the [Trp]>>[^{T1}D] relation does not strictly hold under these conditions. However, at such low Trp concentration, the dominant factors affecting the ^{T1}D concentration are the intrinsic triplet decay and the self dye-quenching mechanisms. Therefore the ^{T1}D concentration can be reasonably estimated even if the pseudo-first order approximation were to fail, as Trp is less influential to ^{T1}D concentration. To further support this argument, we also performed corresponding computations not using the pseudo-first-order approximation (with the Gepasi software package) and showed that the results are very similar (data not shown).

Taking into account the light-intensity attenuation through the NMR sample. In order to take into account the actual optical density of the FL-containing NMR samples used in our experiments, we estimated the extent of light intensity loss as a function of vertical distance ℓ from the tip of the optical fiber (denoting the laser-light origin in the NMR sample) down to the transmitter/receiver coil region of the NMR tube via the Lambert-Beer law

$$I(\ell) = I_o 10^{-\varepsilon [^{S_0}D(t)]\ell} \quad , \tag{45}$$

where ε is the extinction coefficient of the dye, $I(\ell)$ is the irradiance at ℓ, and I_o is the irradiance immediately after optical fiber. Further, we adopt the approximation that the ground-state dye concentration is the same as the initial dye concentration, i.e.

$[^{S_0}D(t)] \cong [D]_{TOT}$. Then

$$I(\ell)=I_o 10^{-\varepsilon[^{S_0}D(t)]\ell} \cong I_o 10^{-\varepsilon[D_T]_O \ell_T} \quad . \tag{46}$$

The excitation rate constant k_{ex} as a function of ℓ can then be computed as

$$k_{ex}(\ell)=\sigma I(\ell) \quad , \tag{47}$$

where σ is the absorption cross section of the dye. Given that the NMR transmitter/receiver-sensitive region of the NMR sample lies ca. 0.5 to 2.5 cm from the light source, corresponding to the value of ℓ, the average steady-state triplet state concentration was estimated according as a simple integration procedure as

$$[^{T_1}D]_{average} = \frac{1}{2.5\text{-}0.5}\int_{0.5}^{2.5}[^{T_1}D](\ell)d\ell \quad . \tag{48}$$

Calculation of triplet-to-singlet mixing rate constant. In the simulations, we estimated the triplet-to-singlet mixing rate constants by noting that the Zeeman term dominates over the hyperfine interaction term in the spin Hamiltonian of the radical ion pair, at high field. We estimated the rate constant for triplet-to-singlet transition rate as

$$k_{mix} \approx \left(g_{FL}\text{-}g_{Trp}\right)\mu_B B_0 \quad , \tag{49}$$

where g_{FL}, g_{Trp} are the g factor of FL and Trp, respectively, μ_B is the Bohr magneton, and B_0 is the external magnetic field, which was set to 14.1 Tesla. The g factor of Trp [5] was set to 2.0027.

Calculation of association and dissociation constants. In order to take into account the diffusive nature of the collision complex and the radical ion pair, we estimated a few key association and dissociation constants based on theoretical considerations. Regarding the association constants pertaining to the interaction of FL with Trp, the coulombic interactions among ions were taken into account via the Debye-Smoluchoski translational-diffusion equation[6-8]

$$k_a = \frac{2kT}{3\eta}\frac{N_a}{1000}\left(\frac{R_{FL}}{R_{Trp}}+\frac{R_{Trp}}{R_{FL}}+2\right)\frac{1}{R_{FT}\int_{R_{FT}}^{\infty} r^{-2}\exp\left(\frac{w(r,I)}{kT}\right)dr} \quad , \tag{50}$$

where k is the Boltzmann constant, T is the temperature, η is the viscosity of the solvent, N_a is Avogadro's number, and R_{FL} and R_{Trp} are hard sphere radii for FL and Trp, respectively (R_{FL} and R_{Trp} are set to 4.4 Å and 4.2 Å, respectively[6]), r is the distance between ions and R_{FT} is the contact distance between FL and Trp, which was set to the sum of R_{FL} and R_{Trp}. Finally, w(r,I) is the coulombic work in an ion-containing solution, which is known to depend on the distance between the ions (r) and the ionic strength I. The ionic strength of the solution was determined according to

$$I=\frac{1}{2}\sum_{p} z_p^2[p] \quad , \tag{51}$$

where [p] is the concentration of p^{th} ions, and z_p is the charge number of the pth ions. In our experiment, the pH was set to 7.0 in a potassium phosphate buffer. Accordingly, the K^+, $(PO_4H_3)^-$, $(PO_4H_2)^{2-}$, H^+ and OH^- ions were taken into account, resulting in an ionic strength of 0.044M. The coulombic work was estimated from Debye-Hückel theory applied to Trp and FL according to[6,7,9]

$$w(r,I)=\frac{z_{FL}z_{Trp}e^2}{2\varepsilon_o\varepsilon_r r}\left(\frac{\exp\left(\beta\sigma_{FL}\sqrt{I}\right)}{1+\beta\sigma_{FL}\sqrt{I}}+\frac{\exp\left(\beta\sigma_{Trp}\sqrt{I}\right)}{1+\beta\sigma_{Trp}\sqrt{I}}\right)\exp\left(-\beta\sigma_{FL}\sqrt{I}\right) \quad , \tag{52}$$

where e is the electron charge, ε_o is the permittivity in vacuum, ε_r is the relative permittivity, r is the distance between two ions, and σ_{FL} and σ_{Trp} are the approximate molecular radii of FL dianion and Trp added to the radii of the dominant counterion within the respective ionic atomosphere[6]. We assumed that σ_{FL} and σ_{Trp} are approximately same as the radii of FL and Trp respectively and values were set to R_{FL} and R_{Trp}, respectivel, and $\beta=\sqrt{\frac{8\pi N_a e^2}{1000\varepsilon_o\varepsilon_r kT}}$.

The dissociation rate constant was calculated as follows from the equation[6,8,10]

$$k_d=\frac{N_a kT}{2\pi\eta R_{FT}^2}\left(\frac{1}{R_{FL}}+\frac{1}{R_{Trp}}\right)\frac{\exp\left(\frac{w(R_{FT},I)}{kT}\right)}{R_{FT}\int_{R_{FT}}^{\infty} r^{-2}\exp\left(\frac{w(r,I)}{kT}\right)dr} \quad . \tag{53}$$

In the case of reduced fluorescein ($FL^{\cdot 3-}$) and $Trp^{+\cdot}$ at room temperature in water (ε_r=78.3 and η=0.91 cp) at ionic strength of 0.044 M, the association constant and dissociation constants were found to be 1.32×10^{10} $M^{-1}s^{-1}$ and 1.52×10^{7} s^{-1}, respectively. For FL and Trp under the same solution conditions, the estimated association and dissociation constant were found to be 7.26×10^{9} $M^{-1}s^{-1}$ and 4.52×10^{9} s^{-1}, respectively.

Estimation of electron transfer rate constants. Since an experimental electron-transfer rate constant (k_{et}) for the reaction between triplet excited-state FL and Trp is not available in the literature, we estimated k_{et} using Marcus theory of electron transfer. According to the Marcus electron transfer equation [6,11-13], intra-molecular electron transfer can be expressed as

$$k_{et} = \frac{4\pi^2 V^2}{h\left(2\pi\lambda kT\right)^{1/2}} \exp\left(-\frac{\left(\lambda + \Delta G_{et}^{o}\right)^2}{4\lambda kT}\right) \quad , \tag{54}$$

where λ is the reorganization energy of electron transfer, which can be divided into solvent (λ_s) and internal reorganization (λ_{int}) energies according to

$$\lambda = \lambda_{int} + \lambda_s \quad . \tag{55}$$

Now, λ_s can be estimated from the dielectric-continuum model by Marcus[14,15] as

$$\lambda_s = \frac{e^2}{4\pi\varepsilon_o}\left(\frac{1}{2R_{FL}} + \frac{1}{2R_{rp}} - \frac{1}{R_{FT}}\right)\left(\frac{1}{n^2} - \frac{1}{\varepsilon_r}\right) \quad , \tag{56}$$

where n is refractive index of water (n_{H2O}=1.33), ε_r is relative dielectric constant of water (78.3), R_{Trp}, R_{FL} are the radii of Trp and FL, respectively, and R_{FT} is the contact distance, which was set to $R_{Trp}+R_{FL}$. For the internal reorganization energy (λ_{int}), same value in Götz et al. and Togashi et al. of 0.42 eV was used in the calculation[6,15,16]. Thus, we obtained the total reorganization energy as

$$\lambda = 0.96 \text{ eV} + 0.42 \text{ eV} \quad . \tag{57}$$

The electronic coupling between FL and Trp was assumed to be similar to the corresponding value for the singlet excited-state of FL and Trp[6] and assigned $V = 0.0021$ eV. The standard-state free energy of photo-induced electron transfer ΔG^o was calculated as

$$\Delta G_{et}^{o} = FE^{o}\left(D^{+\bullet}/D\right) - FE^{o}\left(A/A^{-\bullet}\right) + w\left(D^{+\bullet}A^{-\bullet}\right) - w\left(DA\right) - \Delta E_{S_0 \to T_1} \quad , \tag{58}$$

where F is the Faraday constant, $E^{o}\left(D^{+\bullet}/D\right)$ is the oxidation potential of electron donor, $E^{o}\left(A/A^{-\bullet}\right)$ is the reduction potential of the electron accepter, $w\left(D^{+\bullet}A^{-\bullet}\right)$ and $w\left(DA\right)$ are the coulombic interaction term of the product and reactant of electron transfer reaction, respectively, and $\Delta E_{S_0 \to T_1}$ is the triplet excited energy of the excited molecule. The parameter $E^{o}\left(Trp^{+\bullet}/Trp\right)$ was set to 0.88V[17], and $E^{o}\left(FL/FL^{\bullet -3}\right)$ was set to 0.91V[18] relative to the normal hydrogen electrode (NHE). Coulombic interactions were estimated from Debye-Hückel theory as outlined above eq. (52). We found $w\left(Trp^{+\bullet}FL^{-\bullet}\right) = -0.0638$ eV and $w\left(Trp\ FL\right) = 0$ eV. The triplet excited energy of FL

is $\Delta E^{T} = 2.0241$ eV [19]. We found that $\Delta G^{o}_{ET} = -0.17$ eV. Upon substituting the latter values into eq.(54) we obtained $k_{et} = 2.91\times10^{7}\ s^{-1}$.

In the case of the back-electron transfer reaction, we used eq. (54) with the free energy set to

$$\Delta G^{o}_{bet} = -FE^{o}\left(D^{+\bullet}/D\right) + FE^{o}\left(A/A^{-\bullet}\right) - w\left(D^{+\bullet}A^{-\bullet}\right) + w\left(DA\right) \quad , \qquad (59)$$

and obtained $\Delta G^{o}_{BET} = -1.85$ eV. Upon using the same values employed for forward electron transfer, for reorganization energy and electron coupling term, we obtained the back intra-molecular electron transfer rate constant. $k_{bet} = 2.27\times10^{10}\ s^{-1}$.

Supporting Comments on Processes Leading to Trp and FL Photodegradation

The dominant processes responsible for the photoinduced degradation of FL in the absence of Trp are oxidation by molecular oxygen (dye-to-oxygen or D-O reactions [20,21]) and bimolecular processes between dyes (dye-to-dye or D-D reactions[20,21]). The D-O reactions are allowed to occur if, as previously noted[2], the GO and CAT enzymes do not completely eliminate molecular oxygen in solution. The reaction of FL with $^{3}O_2$ leads to the generation of singlet oxygen $^{1}O_2$, which causes a variety of additional photodegradative processes [22,23]. In the presence of Trp (or other NMR-active molecules of interest), other potential processes may also be involved.

The photodegradation of Trp may result from the generation of singlet oxygen ($^{1}O_2$)[22] in the presence of FL, as outlined in the previous paragraph. In addition, Trp may also be degraded via other unspecified reactions involving the photo-CIDNP dye FL even in the absence of molecular oxygen.

First, to evaluate the overall long-term photostability of FL and FMN (the latter is a conventional photo-CIDNP dye), 1D ^{13}C PRINT photo-CIDNP experiments including several scans were carried out (Fig. 3) in the presence of either FL or FMN at 200 μM $[Trp]_{TOT}$. At this total Trp concentration, we had previously observed that FMN slightly outperforms FL in single-scan experiments (see Fig. 2a-b). Here we notice that the latter trend also applies to multiple-transient experiments up to about 50 scans (Fig. 3). However, after and beyond ca. 50 transients, it is clear that the cumulative Trp-S/N for the data collected in the presence FL exceeds the values obtained in the presence of FMN. At 300 scans, the cumulative Trp S/N in the presence of FL is two-fold higher than that in the presence of FMN. We ascribe this inversion of trend to the fact that either FL is more photostable than FMN, or to the fact that Trp degradation is reduced

in the presence of FL. In summary, the data in Figure 3 show that FL serves as a better photo-CIDNP dye than FMN, over long-term data collection.

Next, the extent of photo-damage of FL and Trp upon laser irradiation was experimentally tested *in situ*. We found that, at 5 μM $[Trp]_{TOT}$ and 6 μM $[FL]_{TOT}$, only an average of 0.5 % photoinactivation per scan takes place, for both Trp and FL (Fig. S5). This conclusion was based on Trp fluorescence and FL electronic absorption measured on samples that has just undergone photo-CIDNP. Despite the progressive inactivation over this long-term data collection, however, the cumulative S/N of Trp keeps increasing steadily even after 80 scans. We deduce that the FL photo-CIDNP sensitizer is compatible with relatively long-term NMR data collection of low-micromolar samples.

Next, we explored the nature of some salient hypothetical photodegradation paths. While little is known in this general area to date, we found it useful to probe the dependence of photodegradation on a few fundamental parameters, to develop a basic instrumental knowledge helpful to guide some of our future experiments. Briefly, the major putative paths for irreversible Trp and FL inactivation, including the D-O and the D-D processes mentioned at the beginning of this section, are schematically shown as gray arrows followed by crosses in Figure S6. As expected from Figure S6, an increase in total Trp concentration should increase the flux through the degradation pathways I and II. Indeed, when we followed the photodegradation of FL (initial total concentration of 6 μM, after eighty 0.1s-laser irradiations) as a function of total Trp concentration (Fig. S7), we noted an increase in FL degradation within the 20-100 μM total Trp concentration range. However, at low total Trp concentrations (0-10 μM), no significant effect is observed. This result suggests that paths belonging to classes I and II are only relevant at high total Trp concentration. On the other hand, within the low-total Trp concentration range of greatest interest to us, these paths are not significant, probably due to the fact that the low $[Trp]_{TOT}$ is not sufficient to lead to any detectable changes in flux through any of the kinetic routes originating from the (^{T1}D Trp) collision complex (see scheme in Fig S6), including the photodegradation routes I and II.

Further insights were provided by additional experiments focusing on the low-[Trp] concentration range. Specifically, we probed the extent of photo-CIDNP and Trp photodegradation as a function of FL concentration (Fig. S8) in samples containing 5 μM total Trp. Panel a of Figure S8 shows that, as the $[FL]_{TOT}$ decreases from 30 to 3 μM, the extent photo-CIDNP increases. The effect is particularly noticeable for a small number of scans. This result is consistent with the kinetic simulations of Figure 5g, showing that the population of the triplet photo-excited dye ^{T1}D (proportional to the

extent of photo-CIDNP) is higher at low total FL concentrations. This effect is desirable, as a high ^{T1}D concentration favors photo-CIDNP. Now, panel b of Figure S8 illustrates the fact that, at the low Trp concentration of 5 μM, the extent of Trp photodegradation is effectively independent of total FL concentration. This result is important because it shows that variations in the ^{T1}D concentration, which stem from changes in the total dye concentration (within the 3-30 μM limit), do not affect the rate of the Trp photodegradation paths II and IV, which are dye-independent. Hence we deduce that paths II and IV are effectively slow compared to the other productive photo-CIDNP-generating paths. Indeed, additional unknown processes, possibly including other reactive species (e.g. superoxide radicals[24]), may be responsible for the observed Trp photodegradation.

In summary, Trp photodegradation pathways are fairly moderate and not dominant in solution, at low Trp and FL concentrations, up to the 80 scan limit tested in this work. Future investigations will be targeted to specifically examine the role of residual molecular oxygen in the NMR samples, and the effect of even longer-term signal averaging.

Supporting References

(1) Mendes, P. Gepasi: A Software Package for Modelling the Dynamics, Steady States and Control of Biochemical and Other Systems. *Comput. Appl. Biosci.* **1993**, *9*, 563-571.

(2) Aitken, C. E.; Marshall, R. A.; Puglisi, J. D. An Oxygen Scavenging System for Improvement of Dye Stability in Single-Molecule Fluorescence Experiments. *Biophys. J.* **2008**, *94*, 1826-1835.

(3) Lee, J. H.; Cavagnero, S. A Novel Tri-Enzyme System in Combination with Laser-Driven NMR Enables Efficient Nuclear Polarization of Biomolecules in Solution. *J. Phys. Chem. B* **2013**, *117*, 6069-6081.

(4) Felix, C.; Weissman, S. Absence of Interference in Photoexcitation of Triplets. *Proc. Natl. Acad. Sci. USA* **1975**, *72*, 4203-4204.

(5) Grosse, S. Cidnp Untersuchungen an Photoinduzierten Radikalpaar-Reaktionen Mit Feldzyklisierung Im Magnetfeldbereich 0 Bis 7 Tesla. Freie Universität Berlin, Germany, 2001.

(6) Togashi, D. M.; Szczupak, B.; Ryder, A. G.; Calvet, A.; O'Loughlin, M. Investigating Tryptophan Quenching of Fluorescein Fluorescence under Protolytic Equilibrium. *J. Phys. Chem. A* **2009**, *113*, 2757-2767.

(7) Sutin, N. Nuclear, Electronic, and Frequency Factors in Electron Transfer Reactions. *Acc. Chem. Res.* **1982**, *15*, 275-282.

(8) Chiorboli, C.; Indelli, M. T.; Rampi Scandola, M. A.; Scandola, F. Salt Effects on Nearly Diffusion Controlled Electron-Transfer Reactions: Bimolecular Rate Constants and Cage Escape Yields in Oxidative Quenching of Tris (2, 2'-Bipyridine) Ruthenium (Ii). *J. Phys. Chem.* **1988**, *92*, 156-163.

(9) Debye, P. Reaction Rates in Ionic Solutions. *Transactions of the Electrochemical Society* **1942**, *82*, 265-272.

(10) Togashi, D. M.; Costa, S. M. Steady State and Dynamic Quenching of Zinc Tetramethylpyridylporphyrin by Methyl Viologen Ion Pairs. Salt Effects. *New J. Chem.* **2002**, *26*, 1774-1783.

(11) Closs, G. L.; Miller, J. R. Intramolecular Long-Distance Electron Transfer in Organic Molecules. *Science* **1988**, *240*, 440-447.

(12) Barbara, P. F.; Meyer, T. J.; Ratner, M. A. Contemporary Issues in Electron Transfer Research. *J. Phys. Chem.* **1996**, *100*, 13148-13168.

(13) Marcus, R. A. On the Theory of Oxidation-Reduction Reactions Involving Electron Transfer. I. *J. Chem. Phys.* **1956**, *24*, 966-978.

(14) Clark, C. D.; Hoffman, M. Z. Effect of Solution Medium on the Rate Constants of Excited-State Electron-Transfer Quenching Reactions of Ruthenium (Ii)-Diimine Photosensitizers. *Coord. Chem. Rev.* **1997**, *159*, 359-373.

(15) Marcus, R. A.; Sutin, N. Electron Transfers in Chemistry and Biology. *Biochim. Biophys. Acta* **1985**, *811*, 265-322.

(16) Götz, M.; Hess, S.; Beste, G.; Skerra, A.; Michel-Beyerle, M. Ultrafast Electron Transfer in the Complex between Fluorescein and a Cognate Engineered Lipocalin Protein, a So-Called Anticalin. *Biochemistry* **2002**, *41*, 4156-4164.

(17) Tommos, C.; Skalicky, J. J.; Pilloud, D. L.; Wand, A. J.; Dutton, P. L. De Novo Proteins as Models of Radical Enzymes. *Biochemistry* **1999**, *38*, 9495-9507.

(18) Compton, R. G.; Mason, D.; Unwin, P. R. Rotating-Disc Electrodes. Single-and Double-Potential Step Chronoamperometry and the Ece–Disp1 Problem. *Journal of the Chemical Society, Faraday Transactions 1* **1988**, *84*, 2057-2068.

(19) Chambers, R. W.; Kearns, D. R. Triplet States of Some Common Photosensitizing Dyes. *Photochem. Photobiol.* **1969**, *10*, 215-219.

(20) Song, L.; Hennink, E.; Young, I. T.; Tanke, H. J. Photobleaching Kinetics of Fluorescein in Quantitative Fluorescence Microscopy. *Biophys. J.* **1995**, *68*, 2588.

(21) Navon, G.; Song, Y.; Room, T.; Appelt, S.; Taylor, R. E.; Pines, A. Enhancement of Solution NMR and Mri with Laser-Polarized Xenon. *Science* **1996**, *271*, 1848-1848.

(22) Connolly, P. J.; Hoch, J. C. Photochemical Degradation of Tryptophan Residues During Cidnp Experiments. *J. Magn. Reson.* **1991**, *95*, 165-173.

(23) Pattison, D. I.; Davies, M. J. Actions of Ultraviolet Light on Cellular Structures. *EXS* **2006**, *96*, 131-157.

(24) Yoshimura, A.; Ohno, T. Lumiflavin-Sensitized Photooxygenation of Indole. *Photochem. Photobiol.* **1988**, *48*, 561-565.

(25) Lee, J. H.; Sekhar, A.; Cavagnero, S. 1h-Detected 13c Photo-Cidnp as a Sensitivity Enhancement Tool in Solution NMR. *J. Am. Chem. Soc.* **2011**, *133*, 8062-8065.

Supporting Figure Legends

Figure S1. Laser irradiation-time dependence of ^{13}C photo-CIDNP. Graphs illustrating how the S/N of the (a) $^{1}H^{\eta 2}$ and (b) $^{1}H^{\alpha}$ Trp resonances varies a function of laser irradiation time in a 1D ^{13}C PRINT photo-CIDNP NMR experiment as a function of laser irradiation time. Experimental conditions and NMR parameters were 5 μM Trp in 10 mM K^{+} phosphate, 5% D_2O,pH 7.0, 25 ^{o}C, catalytic amounts of the GO and CAT enzymes (see Experimental Methods for detail), total FL concentration of 6 μM, 8 scans, argon-ion laser in multiline mode, 1.5 Watt laser irradiation power, Varian Inova 600 MHz NMR spectrometer equipped with a triple-resonance $^{1}H\{^{13}C\text{-}^{15}N\}$ room-temperature probe (see Experimental Methods section for additional details). All experiments were performed in duplicate. Uncertainties were expressed as ± one standard error.

Figure S2. Comparison between the ^{13}C photo-CIDNP of Trp, Tyr and His. ^{13}C PRINT photo-CIDNP for (a)Trp, (b)Tyr and (c)His in the presence (light) and absence (dark) of laser irradiation. 16 scans were collected for all experiments (the laser-on light experiments employed an argon-ion laser in multiline mode at 1.3 W with 0.1 s irradiation time) in the presence of catalytic amounts of the GO-CAT enzyme system (see details in Experimental Methods). These data were collected at 24 ^{o}C on an AVANCE III 600 MHz (14.1 Tesla) NMR spectrometer equipped with a Bruker TBI triple-resonance $^{1}H\{^{13}C, X\}$ z-axis-gradient room-temperature probe. A slightly modified version of the ^{13}C-PRINT pulse sequence [25] was used, with the first 180° pulse replaced by an adiabatic pulse, the total constant-time evolution time T set to 26 ms, and the evolution time τ set to $1/(8J_{CH})$.

Figure S3. Time course of the computationally predicted concentration of triplet-state dye [^{T1}D]. The calculations shown in this figure were carried out for different values of the total dye concentration $[D]_{TOT}$.

Figure S4. Assessment of the validity of pseudo-first-order approximation in the kinetic simulations. Comparison between steady-state values of $[^{T1}D]$ estimated with the Gepasi software package, and the corresponding values obtained after introducing a pseudo-first order approximation evaluated with the MATLAB software package.

Figure S5. FL and Trp photodegradation during photo-CIDNP upon long-term data collection. (a) Plot illustrating the cumulative S/N of dilute (5 μM) aqueous Trp ($^{1}H^{\eta 2}$ resonance) in 1D ^{13}C PRINT photo-CIDNP experiments upon long-term data collection. NMR samples contained 6 μM total FL. All other sample conditions and data acquisition parameters were as in Figure S1, including catalytic concentrations of the GO and CAT enzymes (see Experimental Methods). Cumulative S/N were assessed according to eq. (2). (b) Trp photodegradation monitored via the fluorescence emission intensity of Trp (in NMR samples containing Trp and FL, see details in the legend of Fig. S1) before (I_{-CIDNP}) and after (I_{+CIDNP}) multi-scan photo-CIDNP. Data collection was carried out over multiple scans, as shown in the x axis. Fluorescence emission spectra were collected upon excitation at 280 nm, and emission was assessed at 350 nm. (c) FL photodegradation monitored by electronic absorption at 490 nm (in NMR samples containing Trp and FL, see details in the legend of Fig. S1) before (A_{-CIDNP}) and after (A_{+CIDNP}) multi-scan photo-CIDNP. The very same samples were used to generate the data in panels a, b and c, upon sequential testing by NMR, fluorescence emission and electronic absorption. For every value of photo-CIDNP number of transients, separate fresh samples were used. Two-to-nine experiments were performed for each data point Uncertainties were expressed as ± one standard error.

Figure S6. Scheme illustrating the major kinetic steps involving the photo-CIDNP dye, including the expected photodegradation pathways. Putative photodegradation pathways for FL and Trp are denoted by gray arrows. Generic FL and Trp photodegradation products are marked with a gray cross.

Figure S7. Trp concentration dependence of FL photodegradation. (a) Trp concentration dependence of the ratio of FL absorbance at 490 nm before (A_{-CIDNP}) and after (A_{+CIDNP}) laser irradiation. Experimental conditions and data acquisition parameters were as in Figure S1. Independent experiments were carried out at each Trp concentration. Samples were irradiated 80 times for 0.1 s with a 1.5 W argon-ion laser in multiline mode. Catalytic amounts of the GO and CAT enzymes were included (see Experimental Methods for details). All experiments were performed in duplicate. Uncertainties were expressed as ± one standard error.

Figure S8. FL concentration dependence of Trp and FL photodegradation upon long-term data collection. (a) Plot illustrating the S/N of dilute 5 μM Trp ($^{1}H^{\eta 2}$ resonance) in 1D ^{13}C PRINT photo-CIDNP experiments. Five independent experiments

were carried out at each of the listed total number of scans. 16 experiments were performed to generate each data point and different FL concentrations were analyzed. Laser irradiation parameters were argon-ion laser in multiline mode, 1.5 W laser excitation, 0.1 s laser irradiation time per transient. All other sample conditions and data acquisition parameters were as in Figure S1. Catalytic concentrations of the GO and CAT enzymes were included in the samples. (b) FL concentration dependence of Trp photodegradation monitored via the fluorescence emission intensity of Trp (in NMR samples containing 5 μM Trp and FL) before (I_{-CIDNP}) and after (I_{+CIDNP}) multi-scan (80 transients) photo-CIDNP data collection. Trp fluorescence data were collected as described in Figure S5. The same samples were used to generate the data point in panels (a) and (b). All experiments were performed in duplicate. Uncertainties were expressed as ± one standard error.

Figure S9. Modified version of the plot of Figure 5g. This graph provides a modified version of the plot in Figure 5g where the y axis for the experimental data is normalized S/N, rather than normalized integral. The agreement obtained upon plotting the experimental data as normalized S/N is even better than in the case of normalized integral. Note that at high total dye concentration an experimental S/N of ~ zero was obtained while the normalized-integral measurement yielded a small positive value.

Supporting Figures

Figure S1

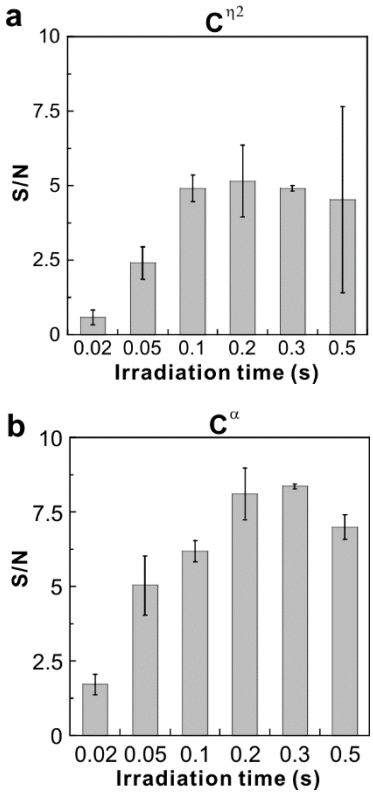

Figure S2

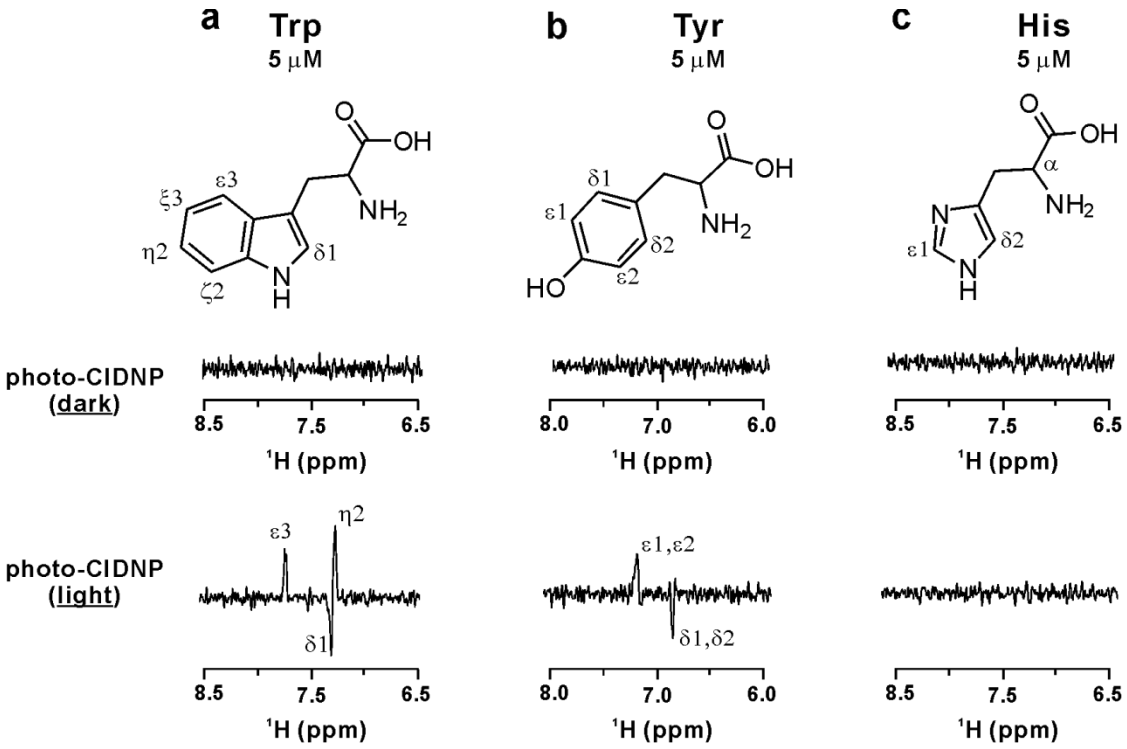
a
Trp
5 μM
b
Tyr
5 μM
c
His
5 μM
photo-CIDNP
(dark)
photo-CIDNP
(light)
ε3
ξ3
η2
ζ2
δ1
ε1
δ2
ε2
α
ε1,ε2
δ1,δ2
8.5
7.5
6.5
8.0
7.0
6.0
¹H (ppm)

Figure S3

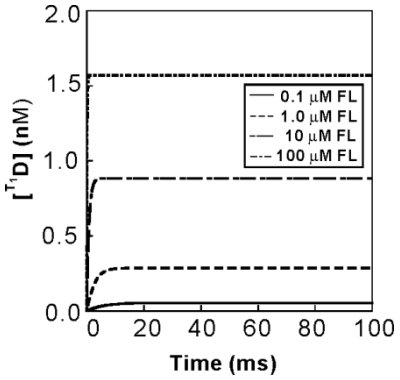
2.0
1.5
1.0
0.5
0.0
0
20
40
60
80
100
Time (ms)
[T1D] (nM)
0.1 μM FL
1.0 μM FL
10 μM FL
100 μM FL

Figure S4

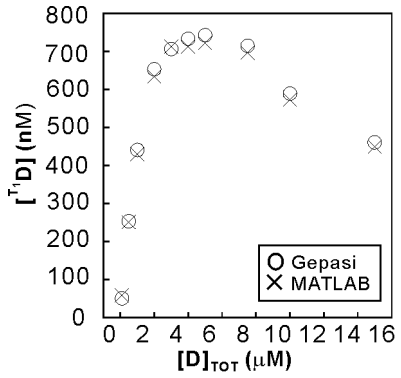
800
700
600
500
400
300
200
100
0
[T1D] (nM)
0 2 4 6 8 10 12 14 16
[D]TOT (μM)
Gepasi
MATLAB

Figure S5

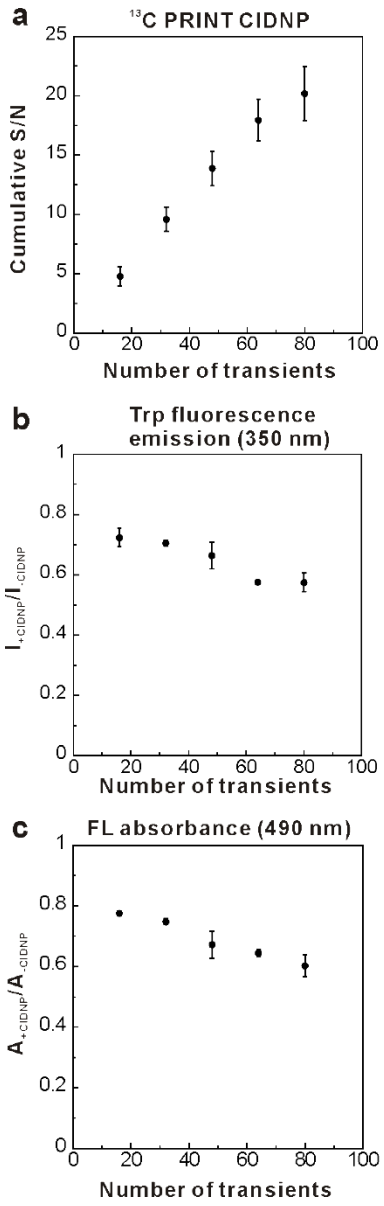
a
^{13}C PRINT CIDNP
Cumulative S/N
Number of transients
b
Trp fluorescence
emission (350 nm)
I_{+CIDNP}/I_{-CIDNP}
Number of transients
c
FL absorbance (490 nm)
A_{+CIDNP}/A_{-CIDNP}
Number of transients

Figure S6

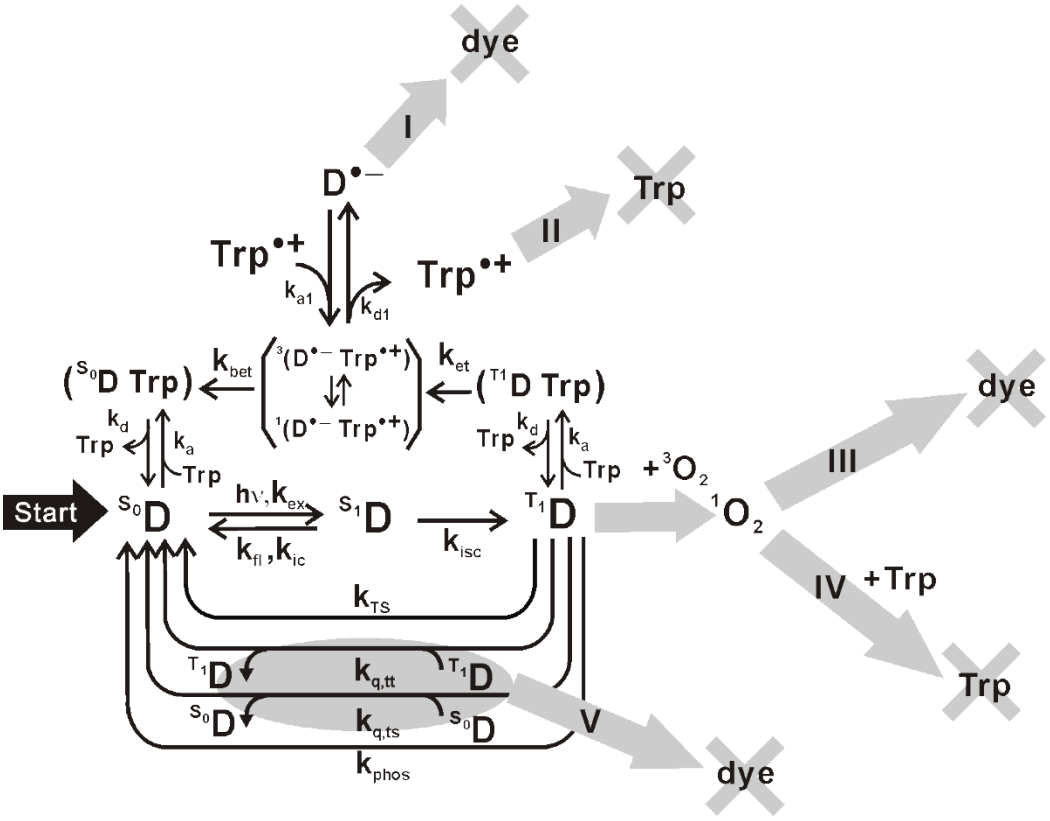
dye
I
D•−
Trp
II
Trp•+
Trp•+
ka1
kd1
(S0D Trp)
kbet
3(D•− Trp•+)
1(D•− Trp•+)
ket
(T1D Trp)
dye
III
kd
Trp
ka
Trp
kd
Trp
ka
Trp
+3O2
Start
S0D
hν, kex
kfl, kic
S1D
kisc
T1D
1O2
IV +Trp
Trp
kTS
T1D
kq,tt
T1D
S0D
kq,ts
S0D
V
kphos
dye

Figure S7

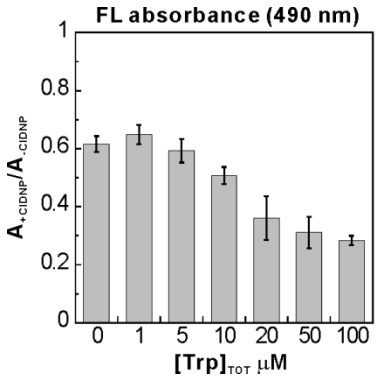
FL absorbance (490 nm)
1
0.8
0.6
0.4
0.2
0
A_{+CIDNP}/A_{-CIDNP}
0
1
5
10
20
50
100
$[Trp]_{TOT}$ μM

Figure S8

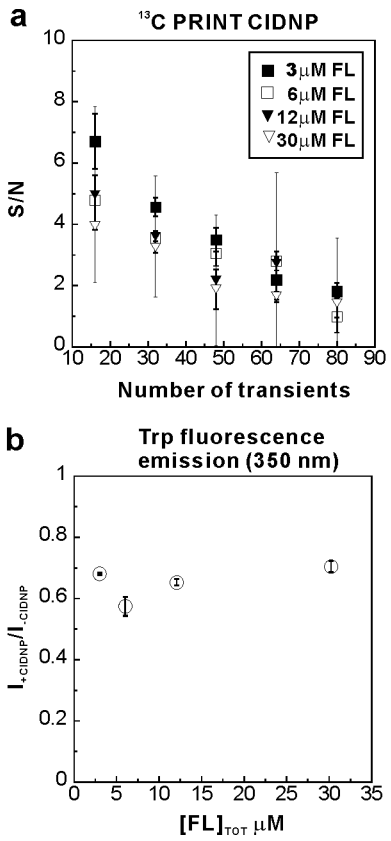
a
^{13}C PRINT CIDNP
3μM FL
6μM FL
12μM FL
30μM FL
S/N
Number of transients
b
Trp fluorescence
emission (350 nm)
I_{+CIDNP}/I_{-CIDNP}
$[FL]_{TOT}$ μM

Figure S9

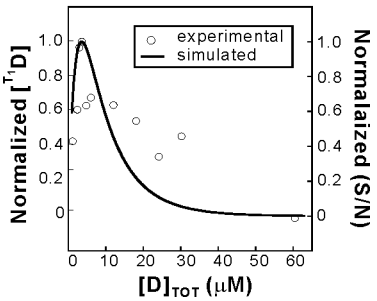
experimental
simulated
Normalized [^{T_1}D]
Normalaized (S/N)
1.0
0.8
0.6
0.4
0.2
0
0 10 20 30 40 50 60
[D]$_{TOT}$ (μM)